Photodetachment of H^- at the GBAR Experiment

Lance Lampert
Advisor: Dr. Pauline Comini

(Dated: August 11, 2023)

I. OVERVIEW OF WORK

The asymmetry of matter and antimatter remains among the most pressing unanswered mysteries in physics. One of the least explored means of probing this asymmetry is through antimatter's interaction with gravity. As antimatter can only be produced and handled in atomic quantities, and gravity is at least 30 orders of magnitude weaker than the electromagnetic force atomic scale, it is an enormous technical challenge to measure this interaction. In fact, no direct measurement of the sign of gravitational acceleration on antimatter has ever been performed [1].

The Gravitational Behavior of Antimatter at Rest (GBAR) experiment, is among a flourishing crop of projects developing at CERN to measure the gravitational acceleration on antimatter, $\bar{g}$ [2]. GBAR aims to measure the value $\bar{g}$ to an accuracy within 1%, with long-term goals to attain accuracy better than .01% [3]. The principle of the experiment is to time the free-fall of cold antihydrogen atoms. $\overline{\mathrm{H}}^+$ atoms are sympathetically cooled with Be^+ in a trap to neV energies, and the excess positron is photodetached from the antihydrogen with a laser, upon which the free-fall begins. The end of the free-fall is marked by the annihilation of the $\overline{\mathrm{H}}$ on the detector, and the value of $\bar{g}$ is calculated from a statistical analysis of many such events.

The measurement of the $\overline{\mathrm{H}}^+$ production cross-section would be a major milestone for GBAR. The GBAR experiment receives a pulsed beam of antiprotons ($\overline{\mathrm{p}}$) from the ELENA decelerator, which are then further slowed to 6 keV and made to interact with a cloud of positronium within GBAR's reaction chamber. GBAR seeks to produce $\overline{\mathrm{H}}^+$ via this interaction through the processes $\overline{\mathrm{p}} + \mathrm{Ps} \to \overline{\mathrm{H}} + e^-$ followed by $\overline{\mathrm{H}} + \mathrm{Ps} \to \overline{\mathrm{H}}^+ + e^-$. So far GBAR has only managed to produce less than one $\overline{\mathrm{H}}$ per hour, which renders the production of $\overline{\mathrm{H}}^+$ currently impossible on reasonable timescales [4], although improvements to GBAR's positronium production scheme are expected to improve this figure significantly. For now, the cross-section for the reaction $\overline{\mathrm{H}} + \mathrm{Ps} \to \overline{\mathrm{H}}^+ + e^-$ has never been measured, and while computational models exist, their predictions for the cross-section vary significantly across different models [5]. Knowing the value of this cross-section will provide crucial information on the rate of production of $\overline{\mathrm{H}}$ necessary for $\overline{\mathrm{H}}^+$ production.

While it is currently impossible to measure this cross-section directly, GBAR is working to measure the cross-section for the charge-conjugated reaction

$$\mathrm{H} + \mathrm{Ps} \to \mathrm{H}^- + e^+, \tag{1}$$

which has the same value as the desired cross-section for the production of $\overline{\mathrm{H}}^+$ (as far as we know). The measurement of this cross-section is much easier because GBAR can (in theory) produce significant numbers of neutral H: as much as six orders of magnitude more per shot compared to GBAR's $\overline{\mathrm{H}}$ production rate in 2022.

The aim of my project was to realize the production of neutral H in-line for the eventual measurement of the cross-section for reaction (1). In addition to antiprotons, ELENA provides a pulsed H^- ion beam to GBAR. Upon entering the reaction chamber, the H^- ions must be photodetached via

$$\mathrm{H}^- + \gamma \to \mathrm{H} + e^-, \tag{2}$$

producing the desired source of neutral H, incident on the Ps cloud. Additionally, these H atoms will first be used for beam alignment, providing a source of neutral atoms which can be used to probe charge buildup and stray electromagnetic fields when compared to the trajectory of the charged H^- beam.

In Section II, I describe the theoretical model I developed to analyze this photodetachment process. In Section III, I investigate my computation of the predicted photodetachment efficiency and results. Finally, in Section IV, I explain the steps I took towards realizing this photodetachment process in the lab.

II. THEORETICAL MODEL OF PHOTODETACHMENT PROCESS

A theoretical model for the photodetachment process given by Equation (2) would provide an upper bound for the photodetachment efficiency of H^-. Such a model would be a useful tool for aligning and determining the necessary operating power of our pulsed 532 nm laser beam.

A diagram of the photodetachment model is shown in Figure 1. A pulsed beam of H^- ions propagate along the y-axis, and our pulsed laser propagates in the xy-plane with angle θ relative to the y-axis. Both beams are assumed to initially have Gaussian profiles and the center of both beams coincide at the origin at time $t = 0$.

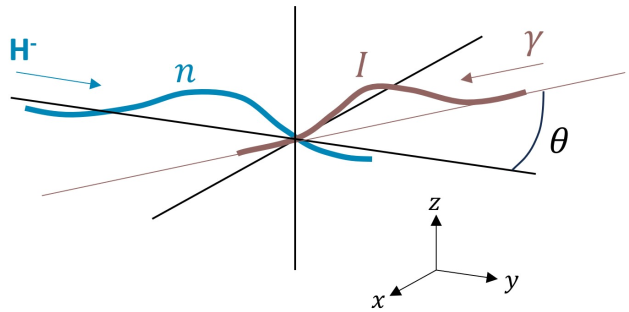

FIG. 1: The photodetachment scheme for some time $t < 0$. A pulse of H^- ions travels in the $+y$ direction while the laser pulse travels in the xy-plane, at angle θ from the $-y$ direction. The Gaussian curves indicate the values of the H^- density n and the beam irradiance I along their respective axes. The two pulses have their centers coincide at the origin at $t = 0$.

In this model $n(x, y, z, t)$ denotes the number density of H^-, and $I(x, y, z, t)$ denotes the irradiance of the pulsed laser. From this model, a partial differential equation was derived for the time-evolution of n:

$$\frac{\partial n}{\partial t} = -\frac{\partial n}{\partial y} v_H - n \frac{I}{E_\gamma} \sigma \tag{3}$$

Here, v_H denotes the speed of the H^- beam, $E_\gamma = \frac{hc}{\lambda}$ is the energy of a photon for the pulsed laser, and σ is the cross-section for the photodetachment of H^-. For GBAR, $v_H = 0.00357c$, $E_\gamma = 2.33\,\mathrm{eV}$ [6][7]. The cross-section σ was taken to be $3.1 \cdot 10^{-17}\,\mathrm{cm}^2$ from [8].

Equation (3) can be understood intuitively. On the right-hand side, the first term, $-\frac{\partial n}{\partial y} v_H$, is taken from the one-way wave equation. It indicates that the ions would propagate in the $+y$ direction at a constant speed v_H in the absence of the pulsed laser. The second term, $-n\frac{I}{E_\gamma}\sigma$, accounts for the photodetachment of H^- into neutral H. Note that $\frac{I(x,y,z,t)}{E_\gamma}\sigma dt$ gives the probability of photodetachment of an H^- located at (x, y, z) between times t and $t + dt$.

Equation (3) is a first-order quasi-linear partial differential equation, and hence can be solved by standard techniques. Utilizing the method of characteristics, a formal expression for the total number of photodetached H^- at $t = \infty$ was derived:

$$N_{\text{detached}} = \int_{\mathbb{R}^3} N_0(x', y', z') \Bigg(1 - \exp\Bigg[- \int_{-\infty}^{\infty} \frac{I(x', y' + v_H t, z', t)}{E_\gamma} \sigma dt \Bigg]\Bigg) dV \tag{4}$$

Here, $N_0(x, y, z)$ is the initial number density distribution of the H^- pulse (at $t = -\infty$), centered at the origin. The volume integral is over all x', y', z'.

Equation (4) can also be explained intuitively. The $(1-\exp[\dots])$ term gives the total photodetachment probability for a H^- located at (x, y, z) relative to the center of the H^- pulse. We then take a sum of this probability over all space, weighed by the number density of H^-.

To be explicit, the full expressions for $I(x, y, z, t)$ and $N_0(x, y, z)$ are

$$\begin{aligned} I &= \left(\frac{2}{\pi}\right)^{3/2} \frac{cE_{\text{pulse}}}{w_0^2 l_0} e^{-2((\alpha^2+z^2)/w_0^2 + (\beta+ct)^2/l_0^2)} \\ N_0 &= \left(\frac{2}{\pi}\right)^{3/2} \frac{N_{\text{bunch}}}{w_1^2 l_1} e^{-2((x^2+z^2)/w_1^2 + y^2/l_1^2)} \end{aligned} \tag{5}$$

where E_{pulse} is the total energy supplied by one pulse of the laser; N_{bunch} is the total number of H^- initially supplied in one pulse; w_0, l_0, and w_1, l_1 are the beam waists and lengths for the laser pulse and the H^- pulse, respectively; and

$$\alpha = x\cos\theta + y\sin\theta, \quad \beta = -x\sin\theta + y\cos\theta$$

are the rotated x, y coordinates for the pulsed laser beam.

For GBAR, we have $w_0 = 6.12\,\mathrm{mm}, l_0 = 1.9\,\mathrm{m}, w_1 = 5.1\,\mathrm{mm}, l_1 = 262\,\mathrm{mm}$, and $N_{\text{bunch}} = 5 \cdot 10^6$, taken from the specifications of our Quantel Laser CFR400 pulsed laser and H^- beam provided from ELENA. We are free to choose E_{pulse} from a few hundreds microjoules to a few hundred millijoules; in Section III we will compute the photodetachment efficiency as a function of E_{pulse}. The beam enters the reaction chamber at an angle of $\theta = 5\pi/6$.

III. COMPUTATION OF PHOTODETACHMENT EFFICIENCY

After deriving Equation (4), I sought to compute N_{detached} over several orders of magnitude of E_{pulse}. Equation (4) cannot be computed analytically, as the $\exp[\dots]$ term introduces a term of the form $e^{e^{f(x,y,z)}}$ (where f is a quadratic polynomial) into the triple integral, which is impossible to integrate analytically in general. Attempts to compute Equation (4) through naive numerical techniques were also unsuccessful. The triple integral would not converge on any reasonable timescale, likely because it was too costly to numerically compute the inner integral on each integrand evaluation.

Therefore, to compute Equation (4), a hybrid approach was taken. As I takes the form of a Gaussian, the inner integral in Equation (4) can be computed analytically.

Then, the analytical form for this integral is substituted into Equation (4), and the triple integral is computed numerically. This was completed in Wolfram Mathematica, because of its ability to perform both analytical and numerical computations natively [9]. To perform the analytical computation, the exponent in the expression for $I(x, y+v_H t, z, t)$ was collected into coefficients of powers of t. These coefficients were then substituted in the form

$$\int_{-\infty}^{\infty} e^{-a_2 t^2 + a_1 t + a_0} dt = \sqrt{\frac{\pi}{a_2}} e^{a_0 - a_1^2/4a_2^2}$$

for a_0, a_1, and a_2. The numerical computation was simply handled by integrating over $-\infty < x, y, z < \infty$ with the built-in `NIntegrate` function.

There also exists background H levels due to collisions of the H^- with gas molecules in the beamline. The background levels were derived from the collision $H^- + H_2 \rightarrow e^- +$ fast H with a cross-section $\sigma = 10^{-15}\,\mathrm{cm}^2$ according to [10]. The number of H atoms produced by this process is $N_{\mathrm{bunch}}(1 - e^{-\sigma x p/kT}) \approx 50$, with $p = 2 \cdot 10^{-9}$ mbar the pressure of the ambient gas, $x = 2.015$ m the length of the relevant portion of the beamline, $T = 293$ K the temperature of the ambient gas, and k Boltzmann's constant. Values were taken from measurements of the GBAR beamline. This estimation is an upper bound, as most background neutral H are produced well upstream in the beamline, and as they cannot be focused, miss any detectors downstream.

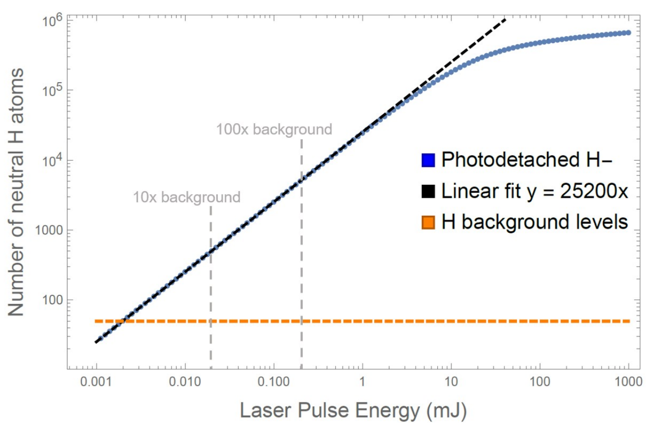

FIG. 2: Calculated levels of H^- photodetachment per shot N_{detached} versus laser pulse energy E_{pulse}. The blue dotted curve gives the calculated values of N_{detached} from Equation (4). The orange dashed line shows the expected background levels of due to collisions with ambient gas in the beamline. The background level was calculated to about 50 neutral H atoms per shot. The black dashed line gives a linear fit for the photodetachment process for small values of E_{pulse} less than a few mJ.

Figure 2 gives the results of the computation over laser pulse energies $1\,\mu\mathrm{J} < E_{\mathrm{pulse}} < 1\,\mathrm{J}$. For pulse energies less than a few millijoule, the photodetachment efficiency closely follows a linear relationship in pulse energy, which is to be expected below saturation energies.

Recall the neutral H beam will be used in two contexts: for beam alignment and for measurement of the antihydrogen ion production cross-section. These two contexts will require different energy scales. For beam alignment, we only need one or two orders of magnitude of neutral H produced above background levels, which according to Figure 2, corresponds to less than 0.2 mJ per pulse. For the measurement of antihydrogen ion production cross-section, we would like as much neutral H produced as possible, so we plan to operate within the saturation region, $E_{\mathrm{pulse}} \sim 50\,\mathrm{mJ} - 100\,\mathrm{mJ}$.

This photodetachment model is flexible. Beam delays and offsets can be included into the model without changing the form of the formal solution (Equation (4)) or the computations. Therefore, this model can also be used to study the effect of misalignment and mistiming of the laser beam on photodetachment efficiency with very little additional effort. This was not pursued in this project.

One flaw of this computational method is that it assumes that $I(x, y, z, t)$ can be integrated analytically. This may not always be the case if, for example, a portion of the beam is cut off. In this case, one must return to numerical methods. One possibility is to pre-compute $F(x, y, z) = \int_{-\infty}^{\infty} I(x, y + v_H t, z, t) dt$ on a discrete grid on which the integral evaluates to a non-marginal value. Then, $F(x, y, z)$ can be extended to all of $\mathbb{R}^3$ via interpolation, which will allow for the numerical computation of the outer triple integral, without evaluating the inner integral on each integrand evaluation. The resolution of this discrete grid and the range of values to evaluate $F(x, y, z)$ may be determined manually or by an algorithm. This was not pursued in this project.

IV. EXPERIMENTAL REALIZATION OF PHOTODETACHMENT

A. Alignment of laser

Our source of the photons for photodetachment is a CFR400 high-powered pulsed Nd:YAG laser operating at 532 nm. As a Class 4 laser, the CFR400 cannot be located directly in the experimental zone, and is instead located in an isolated room above the reaction chamber. To direct the beam into the reaction chamber, it must be aligned through a three-meter tube to the experimental zone and directed into the reaction chamber at a 30° angle. The alignment was initially completed with a low-powered diode laser before aligning the high-powered pulsed laser.

The alignment process turned out to be more difficult than initially anticipated; the laser had been aligned a few years prior, but after a week of work, I was convinced the beam could not be aligned through the three-meter tube given the existing placement of the optics. Following my observations, my advisor, Dr. Comini, later realized that the tube had been shifted a few centimeters during the installation of an iron shielding around the reaction chamber, rendering alignment impossible. After repositioning the existing optics, I successfully managed to direct the diode, and then the high-powered beam, from the laser room down to the experimental zone. An endoscope was used to identify and eliminate the deflections of the laser within the tube, and a camcorder was used to remotely view the path of the laser in the experimental zone while optics were adjusted in the laser room (and vice versa). The beam path of the laser is shown in Figure 3.

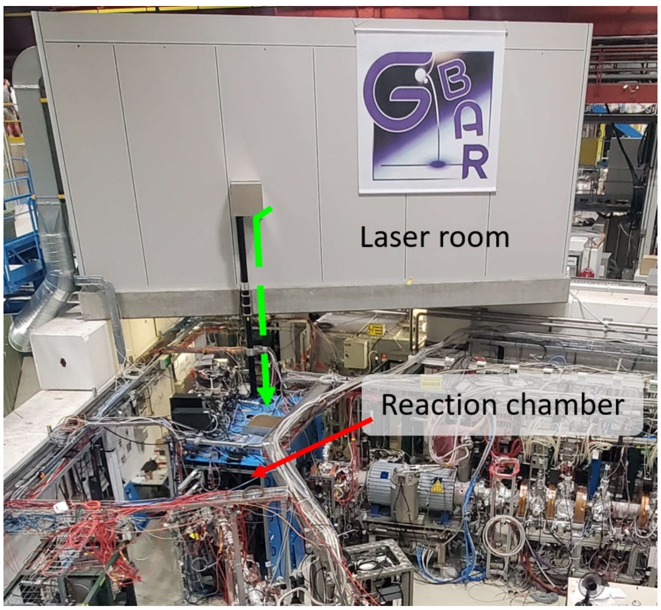

FIG. 3: The path of the CFR400 pulsed laser beam. The CFR400 is located inside the laser room above, and is directed down a three-meter tube to the reaction chamber, where it photodetaches incoming H^- ions. The path of the beam is indicated by the dashed green arrow, and the reaction chamber is obscured under the iron shielding.

B. Detection of laser transmission

Figure 4 displays the beam path of the pulsed laser through the reaction chamber. The laser exits the reaction chamber 30° below horizontal. In order to correctly time the laser pulses with the H^- beam (see Section IV C), as well as confirm successful transmission through the reaction chamber, it would be useful to detect the transmission at this exit port. Moreover, the high-powered beam must be absorbed at this exit port by a beam-block.

While we had access to a photodiode and a beam-block, due to the beam block being in a very cramped space, mounting these two components to the exit port arose as a challenge. We decided the best way to proceed would be to design a 3D printed support, which would be held by the exit port and a nearby metal beam. I designed the support in Autodesk Inventor, and printed the design at the CERN IdeaSquare. This was the first time I had used CAD software to design and print a 3D model. The design and installation of the beam-block assembly is shown in Figure 5.

Currently, the assembly supports its own weight thanks to the additional stability provided by the metal support beam. However, given a small external force, the assembly can easily be perturbed. While this is not an urgent issue, if the assembly is not positioned correctly, part of the high-powered beam will not enter the beam-block and will not be properly absorbed. In a future iteration of the beam-block support, three design changes would serve to provide more stability to the structure:

1. Double or triple the thickness of the component that attaches to the metal support beam. Currently, this component is much too flexible.

2. Add a second screw for the metal support beam. Currently, the assembly can rotate about the single screw attached to the metal beam, even when tightened. Adding a second screw along the beam should serve to prevent this rotation.

3. Decrease the tolerances and increase the thickness of the circular hole at the end of the support. This will provide less freedom for the support to rotate relative to the viewport angle.

C. Timing of laser trigger

The final step in preparing for photodetachment of H^- is to time the CFR400 laser pulse to arrive in the reaction chamber at the same time as the H^-. By having the peaks of both beams coincide, we maximize our photodetachment efficiency.

GBAR receives a low-jitter trigger from ELENA about 1 ms before the arrival of a H^- pulse in the reaction chamber. The CFR400 is optically pumped by a flashlamp, which takes approximately 173 µs to reach peak fluorescence after receiving an external trigger signal [11]. Upon reaching maximum fluorescence, the laser must be Q-switched. While this 173 µs delay can be programmed

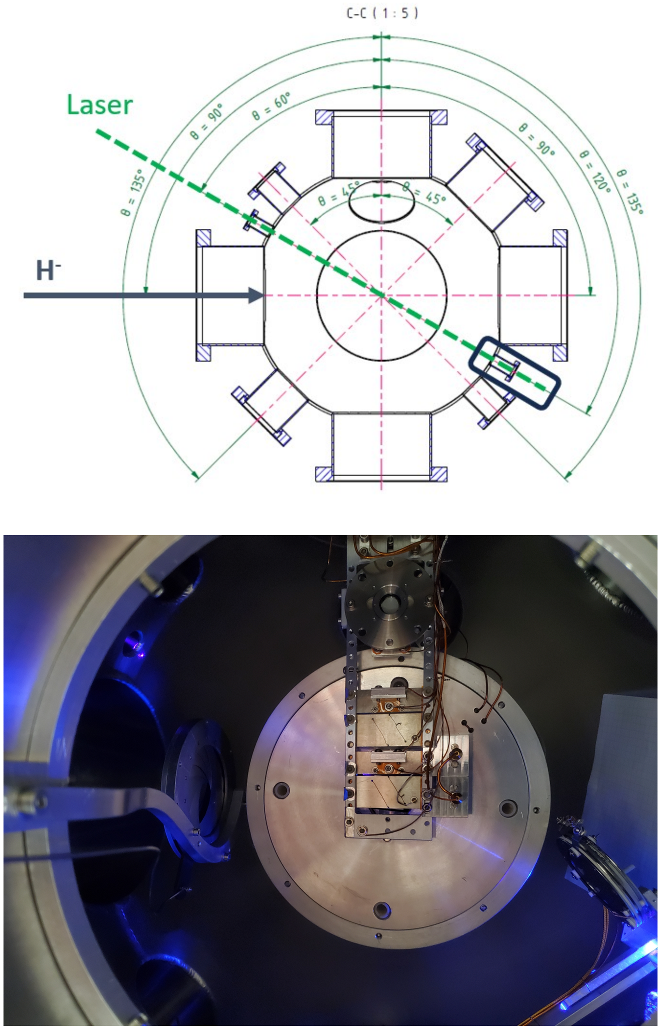

FIG. 4: Top: A schematic diagram of the reaction chamber. The chamber is 40 cm in diameter. The laser beam (indicated by the dashed green line) enters at a 30° angle to the horizontal and interacts with the incoming H^- beam at the center of the chamber, just in front of the Ps cloud. The exit port for the laser is circled at the bottom right. This is the location of the photodetector and beam-block assembly shown in Figure 5. The entry and exit ports for the laser are 16 mm in diameter. **Bottom:** A picture of the inside of the reaction chamber with a blue diode laser used for alignment. The beam enters from the top left port and exit through a port on the bottom right (not shown). The photodetachment occurs in the center of reaction chamber, behind the target holder.

internally, we found the internal delay jitter to be too large for our applications, on the order of 100 ns. Therefore, two external triggers are required for the CFR400: one for the flashlamp, one for the Q-switch. These triggers are both sourced from the −1 ms ELENA trigger.

A diagram of the trigger signal line is shown in Figure 6. Two delay generators are used to generate the triggers for the flashlamp and the Q-switch. While it would be possible to generate both trigger signals directly from the DG645 delay generator, only one channel is available for use. The TG5011, which we acquired from the CERN electronics pool, is also a single-channel function generator.

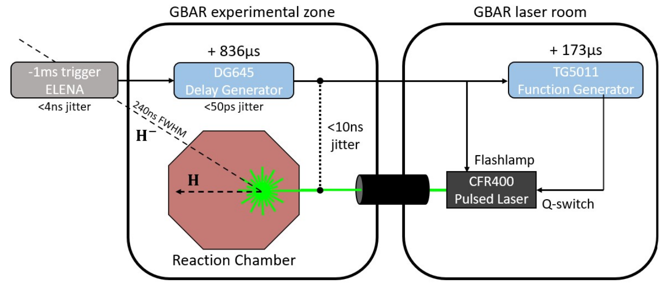

FIG. 6: The signal line for the laser trigger. The −1 ms trigger from ELENA is triggered by ejection of the H^- from the ELENA ring. The signal is then fed to a DG645 delay generator, whose output is split to the flashlamp and the external trigger of a TG5011 function generator. The TG5011 output is fed to the Q-switch of the CFR400 laser, which is then directed to the reaction chamber on the incoming H^- ions to create neutral H.

The delay value for the TG5011 function generator (see Figure 6) is fixed to the 173 µs delay between the flashlamp trigger and peak fluorescence. The initial delay value for the DG645 was calculated, accounting for delays in the transmission of the signal as well as internal delays in the two delay generators and the pulsed laser. Fine-tuning of the DG645 delay was accomplished by comparing the timing of the signal from the photodiode pickup described in Section IV B and a fast Lead Tungstate scintillator picking up the annihilation of antiprotons at the end of the reaction chamber [12]. The total jitter from the start to the end of the signal line is less than 15 ns, which is sufficient for our needs, as the H^- beam has a Full-Width-Half-Maximum (FWHM) of 240 ns.

Figure 7 displays the fine-tuned timing of the laser pulse relative to the Lead Tungstate signal from the annihilation of the $\bar{p}$ beam. This oscilloscope reading demonstrates:

1. The high-powered beam is successfully transmitting from the laser room to the reaction chamber and through the exit viewport, as described in Section IV A; we see a significant signal on the photodiode (C4).
2. The laser is being detected and absorbed at the exit viewport, as described in Section IV B. We know the laser is being absorbed because the photodiode signal is well below saturation.
3. The timing of the laser beam has been adjusted to coincide with the H^- pulse, as described in Sec-

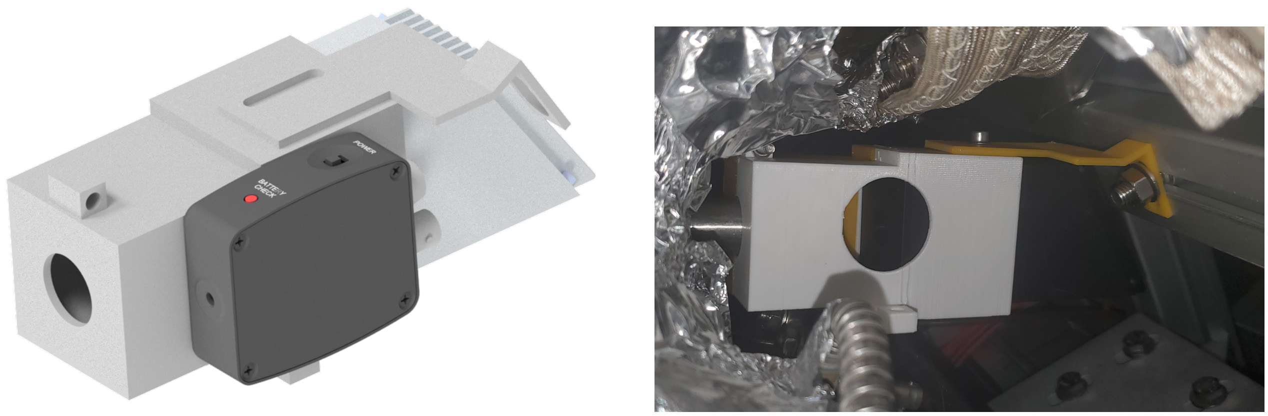

FIG. 5: Left: A 3D render of the beam-block assembly design. The photodiode is held from the side via a screw, and the beam-block from the top. The 3D printed support is composed of three components, two which wrap around the exit viewport and are held together via two screws, and one which screws down to a metal beam to provide more stability to the structure. **Right:** The beam-block assembly as installed at the exit viewport of the reaction chamber. The metal support beam can be seen to the right of the image. The photodiode is removed during alignment of the low-powered laser.

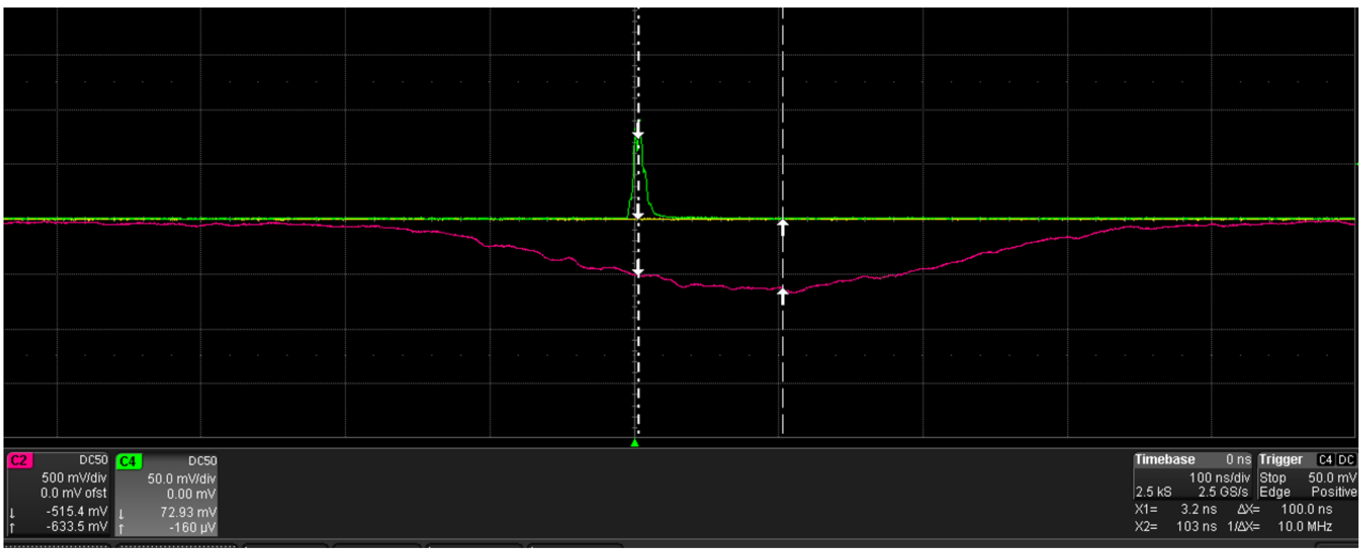

FIG. 7: The timing of the laser pulse against the timing of the H^- beam arrival. The photodiode signal at the exit viewport of the pulsed laser path is shown in green (C4). The sharp peak corresponds to the laser pulse arriving on the photodiode. The purple signal (C3) corresponds to the lead tungstate scintillator placed outside the reaction chamber. Although the signal is quite broad, we tuned the timing of the laser pulse so that there is approximately a 100 ns delay between the laser pulse arrival and the peak of the scintillator signal.

tion IV C. The roughly 100 ns delay between the laser pulse and the peak of the scintillator signal accounts for the 10 cm between the crossing of the laser pulse and the H^- beam and the annihilation position of the $\bar{p}$. In any case, because the scintillator signal is so broad, this will need to be further adjusted after measurements of H^- photodetachment are completed.

On the last day of my project we obtained visual confirmation of the successful photodetachment of H^- , which is displayed in Figure 8. This figure is the culmination of the work described in Section IV. Following photodetachment, the remaining H^- ions were diverted from the beam path using a high-voltage deflector about 3 cm downstream from the photodetachment location. Only the neutral H remain on the beam path, and are detected by a microchannel plate detector (MCP) about 10 cm from the photodetachment position. This is the same MCP that we use to detect $\bar{H}$; see [4] for a description of the MCP.

The number of neutral H detected is less than predicted for both the background and photodetachment. As for the background, this is likely because most of the background H atoms are produced relatively far upstream, and as they cannot be focused, they miss the MCP. For the photodetachment measurement, this is caused by several factors. Primarily, the beam alignment still needs to be optimized, but we did not have time for this before my project concluded.

Finally, one loose end: I designed and prototyped a voltage adder circuit. The circuit is designed to drive a $50\,\Omega$ load at up to $\pm 15\,$V. A diagram of the circuit is shown in Figure 9. The primary component of the circuit is a LT1206 op-amp, designed to supply up to 250 mA of current, which is necessary to drive a low-impedance load. The LT1206 was also selected for its fast slew rate, to match the CFR400 trigger requirements of $< 1\,\mu$s rise time. This circuit has been demonstrated to work as intended on a breadboard, but has not yet been permanently installed beyond this.

This circuit was initially designed to comply to a compulsory 2-second "warm up" period between the flashlamp activiation and Q-switching on the CFR400. This would require two signals (a series of pulses for the warming-up of the flashlamp, and a single pulse for the precise final flashlamp activation) to be summed into the external flashlamp trigger of the CFR400. However, we managed to disable this "warm-up" setting, so we proceeded with the signal line given in Figure 6. We will instead apply this circuit within a different application: the excitation of positronium, which is beyond the scope of this project.

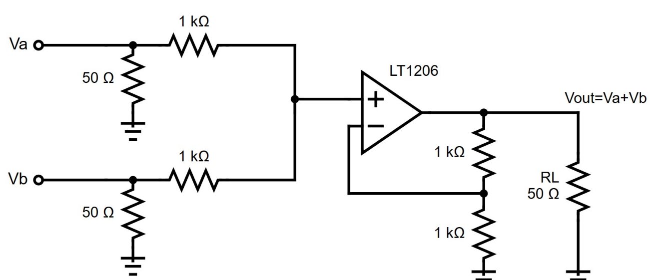

FIG. 9: The voltage adder circuit design. The voltage sources V_a and V_b are assumed to be designed to drive a $50\,\Omega$ load.

V. SUMMARY AND OUTLOOK

The GBAR experiment aims to measure the gravitational acceleration on antimatter, $\bar{g}$. A crucial step to realizing this goal is the production of $\overline{\mathrm{H}}^+$ atoms through the reaction $\overline{\mathrm{H}}+\mathrm{Ps} \rightarrow \overline{\mathrm{H}}^+ + e^-$, which does not have a precisely known cross-section. To measure this cross-section, GBAR seeks to measure the cross-section for the charge-conjugated reaction, reaction (1). GBAR is provided a source of H^- ions from ELENA, so it is first necessary to photodetach these ions in-line (reaction (2)) before they interact with positronium. A neutral beam of H atoms will also be useful for beam diagnostics and alignment. The aim of my project was to experimentally realize the photodetachment of H^- in the GBAR experiment.

A theoretical model for the photodetachment was developed, and simulations of the photodetachment process were run to better understand how the photodetachment efficiency depends on the pulsed laser beam energy. To achieve photodetachment an order of magnitude or two greater than background H levels, the beam needs to be run at less than 1 mJ. The photodetachment efficiency closely follows a linear relationship with the beam energy for energies less than a few millijoule, and at maximum operating power, the beam energy is well within the saturation region.

Experimentally realizing the photodetachment of H^- proceeded in three steps. First, the laser beam was aligned from the laser room to the reaction chamber. Then, a beam-block assembly was printed and assembled to absorb and detect the beam at the exit port of the reaction chamber. Lastly, the trigger timing for the pulsed laser flashlamp and Q-switch was tuned so that the laser beam arrives in the reaction chamber on the incoming H^- ions. We observed the successful photodetachment of H^- ions in the reaction chamber via an MCP detector located downstream in the beamline, achieving the goal set out at the start of the project.

To make further developments, the beam alignment and timing should be optimized. This should be sufficient for developing a neutral beam for beam diagnostics. For measurement of the cross-section of reaction (1), further work will be required. For one, the H^- ions will have to be photodetached slightly earlier in the beam-line; currently they are being photodetached where the Ps cloud will be located, and this will make it impossible to isolate the H^- produced by reaction (1). Moreover, we would like to photodetach as many H^- as possible for this process. As the H^- beam's length is considerably larger than laser beam width, it would be beneficial to redirect the laser beam through the H^- beam several times, which would required the installation of new optics in the reaction chamber. The simulated photodetachment model can be adjusted accordingly to estimate the expected H^- photodetachment with this proposed method. We hope to obtain a measurement of the cross-section for reaction (1) in 2024.

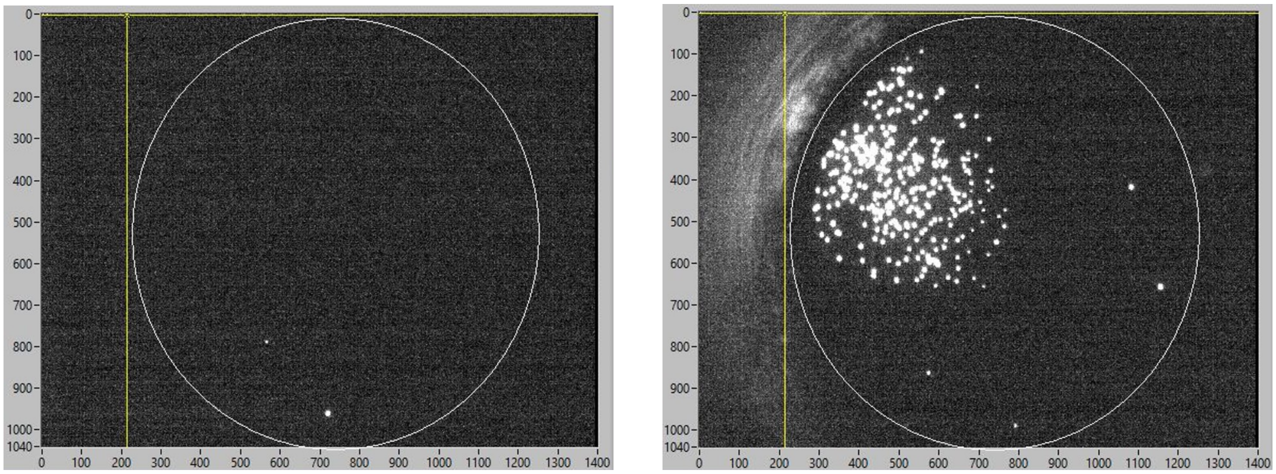

FIG. 8: Visual confirmation of H^- photodetachment. The two images are taken from a MCP downstream from the photodetachment location. The white dots correspond to the detection of a neutral H atom on the MCP. **Left:** The background levels of neutral H detected. Background measurements were achieved by turning off the pulsed laser, in which case the only neutral *H* produced is the background. **Right:** The preliminary photodetachment levels. This is what is observed on the MCP with the pulsed laser on.

[1] Olivier Rousselle, Pierre Cladé, Saïda Guellati-Khelifa, Romain Guérout, and Serge Reynaud. Analysis of the timing of freely falling antihydrogen. *New Journal of Physics*, 24(3):033045, mar 2022.

[2] G. Chardin et al. (GBAR collaboration). Proposal to measure the Gravitational Behaviour of Antihydrogen at Rest. 9 2011.

[3] P.-P. Crépin, C. Christen, R. Guérout, V. V. Nesvizhevsky, A.Yu. Voronin, and S. Reynaud. Quantum interference test of the equivalence principle on antihydrogen. *Phys. Rev. A*, 99:042119, Apr 2019.

[4] P. Adrich et al. (GBAR collaboration). Production of antihydrogen atoms by 6 kev antiprotons through a positronium cloud, 2023.

[5] Takuma Yamashita, Yasushi Kino, Emiko Hiyama, Svante Jonsell, and Piotr Froelich. Near-threshold behavior of positronium-antihydrogen scattering cross sections. *Phys. Rev. A*, 105:052812, May 2022.

[6] D. Lunney et al. (GBAR collaboration). AD-7/GBAR status report for the 2023 CERN SPSC. Technical report, CERN, Geneva, 2023.

[7] Note the H^- beam is nonrelativistic, so there is negligible Doppler shift of the pulsed laser wavelength, but for high-energy beams this must be taken into account when calculating E_γ.

[8] A. P. O'Connor, F. Grussie, H. Bruhns, N. de Ruette, T. P. Koenning, K. A. Miller, D. W. Savin, J. Stützel, X. Urbain, and H. Kreckel. Generation of neutral atomic beams utilizing photodetachment by high power diode laser stacks. *Review of Scientific Instruments*, 86(11):113306, 11 2015.

[9] One could possibly compute the analytical integral by hand, but the coefficients in the exponent for I are quite messy.

[10] Tatsuo Tabata and Toshizo Shirai. Analytic cross sections for collisions of h+, h2+, h3+, h, h2, and h- with hydrogen molecules. *Atomic Data and Nuclear Data Tables*, 76(1):1–25, 2000.

[11] Depending on the operating mode, this delay may instead be 673 µs, but the same principles apply.

[12] Recall GBAR receives both a H^- beam as well as an antiproton beam from ELENA. The dynamics of both beams are essentially the same, so they can be used interchangeably for this purpose. In this case, it is more convenient to use antiprotons because their annihilations are easier to detect.